

PSF engineering with variable logarithmic phase plates for the extended depth of field

SARA MOEIN, D SHOHREH SHADALOU, AND THOMAS J. SULESKI

Department of Physics and Optical Science, University of North Carolina at Charlotte, Charlotte, NC 28223, USA

Abstract: Shallow depth of field in imaging systems with high numerical apertures results in images with in- and out-of-focus regions. Therefore, methods to enhance the depth of field are of special interest. In point spread function engineering, a custom phase plate is designed for each system to reduce sensitivity to defocus and thereby extend depth of field. In this paper, we present a method that enables extended depth of field for a range of numerical apertures using a freeform variable logarithmic phase plate pair. We leverage a numerical design approach for the variable phase plate pair design, and explore phase plate optimization and performance by quantifying and comparing through-focus point spread function variation, and on- and off-axis performance for the designed phase plates.

© 2022 Optica Publishing Group under the terms of the Optica Open Access Publishing Agreement

Introduction

The minimum lateral distance that an optical imaging system can resolve (the Rayleigh resolution) is inversely proportional to system Numerical Aperture (NA) [1], and the axial distance in object space over which the optical system creates an in-focus image of the object, the Depth of Field (DoF), is inversely proportional to the square of NA [2]. With increases in system NA and magnification, the lateral resolution is improved while the DoF becomes shallow; therefore, methods that enable Extended DoF (EDoF) while maintaining system NA are beneficial. DoF is defined in the object space, but the expression has been used to study spot and Point-Spread Function (PSF) variation in the image space (depth of focus), and we follow similar terminology throughout this work.

PSF engineering has provided powerful methods to modify transmitted wavefronts to reduce sensitivity to defocus and thus enable EDoF [3]. In PSF engineering, a custom phase component is placed at or near the system exit pupil and computational methods are then used to retrieve sharper images. A wide range of phase elements with rotationally symmetric [4–11] and asymmetric [12–20] surface profiles have previously been used to enable EDoF. For these applications, a specially designed component is required for each system. Thus, methods with the potential to enable EDoF for multiple imaging systems with the same phase element or elements can be advantageous.

The concept of creating variable wavefronts through relative movement between two identical components has been previously reported for multiple applications, including variable power lenses [21–26], aberration correction [27–29], tunable illuminators [30] and beam shaping [31,32], among others. For variable EDoF, the two phase plates are translated or rotated relative to each other to create a focus-invariant PSF. Examples include shifted and rotated polynomial, sinusoidal, hyperbolic and gaussian mask pairs for applications such as barcode readers, microscopy and 3D imaging [33–40].

We have previously reported on the design of Quartic Phase Plate Pairs (QPPP) to enable EDoF for aspheric singlets with different NA values [41] based on Cubic Phase Plate (CPP) designs [42]. In this approach, fixed CPPs were designed for the selected lenses and then an analytical

^{*}smoein@uncc.edu

approach [27] was used to derive the surface equation and calculate the surface coefficient of the QPPP and the required shifts to match the NA for each lens.

Logarithmic Phase Plates (LPP) have been previously reported to enable EDoF over larger ranges of defocus compared to CPP [13]. This result provides motivation for our study on the design and performance of Variable Logarithmic Phase Plate Pairs (VLPPP) to further extend DoF for lenses with different NA values through relative translation of VLPPP components, in a manner analogous to the prior work on QPPP [42]. The general surface form of the LPP is given in Eq. (1) [13]:

$$z(x, y) = \operatorname{sgn}(x)\alpha x_{\max}^2 x^2 (\log|x| + \beta) - \frac{u' x_{\max} x}{z_i} + \operatorname{sgn}(y)\alpha y_{\max}^2 y^2 (\log|y| + \beta) - \frac{v' y_{\max} y}{z_i}.$$
 (1)

In this equation, α and β are logarithmic parameters, x_{max} and y_{max} are half-widths of the aperture, (u',v') is an arbitrary point in the image plane, and z_i is the image distance. The LPP and VLPPP components are plano-freeform configurations placed at or near the exit pupil of the optical system, as illustrated in Fig. 1 for aspheric singlets.

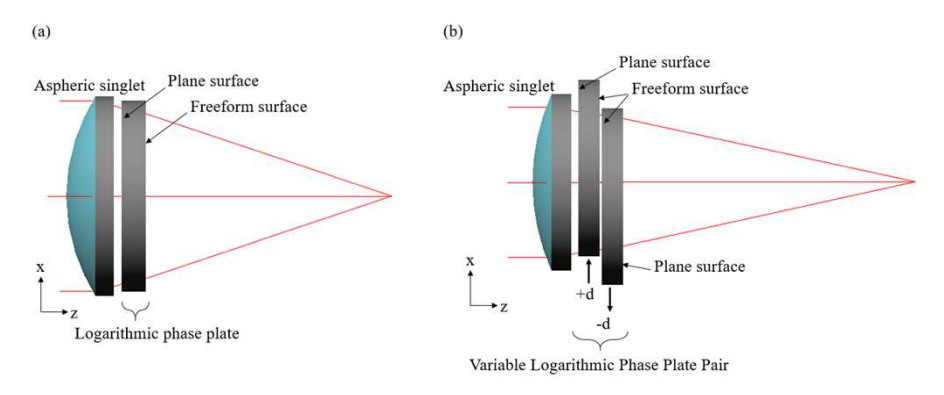


Fig. 1. Schematic of a 0.25 NA aspheric lens with (a) LPP and (b) VLPPP.

We note that the nature of the LPP surface descriptions necessitates a different design approach than previous work from [42]. In particular, the analytical design method used to derive the form of the QPPP from CPP is not conducive for the present work on logarithmic phase plates; as a consequence, a numerical design approach must be implemented to find the desired VLPPP surfaces [43]. We consider the EDoF capability of the resulting logarithmic phase plates by comparing both through-focus spot diagrams (ray-based models) and PSFs (wave-based models). The analyses of the LPP and VLPPP elements parallel the treatment of the CPP and QPPP systems in Ref. [42] to enable direct comparison of the two geometries.

Design approach and results

For this design, three Commercial-Off-The-Shelf (COTS) aspheric singlets with 0.25, 0.33, and 0.50 NA values and 22.5 mm Clear Aperture (CA) are considered [41]. CODE V and MATLAB were used for optical design and performance analysis. A schematic illustration of the design procedures for the LPP and VLPPP components is shown in Fig. 2.

First, the LPP form is implemented in CODE V. CODE V supports a wide range of surface profiles for implementation, however, the logarithmic form of Eq. (1) is not supported and therefore, a User-Defined surface is required [44]. Next, the LPP surface coefficients are optimized in CODE V for all lenses. The LPP designs for the 0.25 and 0.50 NA lenses are then used as boundary elements in MATLAB as part of a numerical design process to realize point-cloud representations of the VLPPP elements [43]. The resulting VLPPP surface point

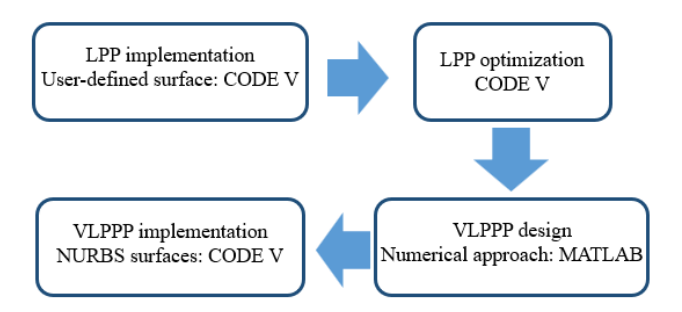


Fig. 2. Summary of the LPP and VLPPP design process.

clouds are next imported into CODE V as User-Defined NURBS surfaces, where they can be used to model the desired EDoF functionality across the range of NA values. We now consider each of these design stages in more detail.

2.1. Logarithmic phase plate design and optimization

As shown in Fig. 1(a), the LPPs are in a plano-freeform configuration located near the exit pupil of the aspheric singlets. However, due to inaccessibility of the exit pupils for the selected lenses and optomechanical considerations, the air gaps between the aspheric lenses and phase plates were set to 1 mm. The LPPs are designed from Polymethyl Methacrylate (PMMA) at a design wavelength of 633 nm (refractive index n = 1.489) with 22 mm clear aperture and 3 mm center thickness.

The LPP was implemented in CODE V using Eq. (1) and its derivative to create a user-defined surface for use in optimizing the performance of the EDoF system [44,45]. The design goal is to create spots that are insensitive to defocus over a range from $-6\Delta z$ to $+6\Delta z$, where:

$$\Delta z = \frac{n\lambda}{NA^2},\tag{2}$$

where n is the refractive index of the surrounding medium (n = 1 for air), λ is the design wavelength and NA is the lens numerical aperture [1]. The variable parameters for the LPP design are the α and β coefficients in Eq. (1); u', v' and z_i are neglected due to their negligible effect on phase plate performance [13,18].

Following the method of Ref. [42], the optimization routine satisfies two MTF-based performance requirements to achieve EDoF imaging. First, to improve the performance of each system by increasing through-focus MTF values at specific spatial frequencies, and second to decrease through-focus performance variation by minimizing the MTF value differences for the selected spatial frequencies. The optimization frequencies were selected by identifying the specific frequency ranges exhibiting low values in the through-focus MTF performance of each lens, and directly implemented in the merit function. The selected spatial frequencies for each aspheric lens are summarized in Table 1.

Table 1. Optimization frequencies used to design LPPs for the selected aspheric lenses.

| Lens NA | Optimization spatial frequencies (cycles/mm) | |
|---------|--|--|
| 0.25 | 60, 86, 124, 240 | |
| 0.33 | 61, 98, 115, 270 | |
| 0.50 | 80, 160, 320, 480 | |

Three LPPs were designed based on the described criteria, one for each aspheric lens. Table 2 summarizes the surface parameters and sags of each design. Figure 3 shows 3D plots for the surface of the LPPs designed for the 0.25 and 0.50 NA lenses.

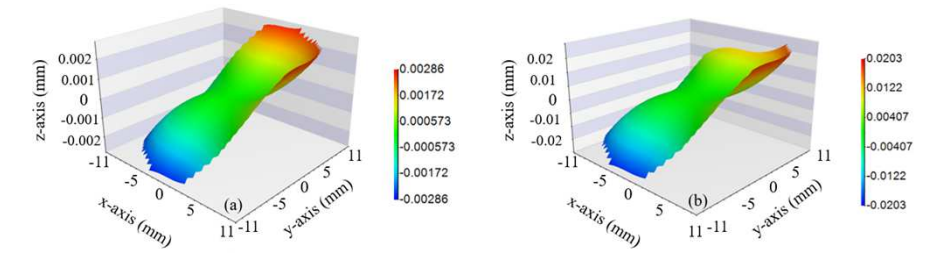


Fig. 3. 3D surface map for the LPPs designed for (a) 0.25 and (b) 0.50 NA lenses over 22 mm clear aperture.

Table 2. LPP surface coefficients and sags for lenses with 0.25, 0.33 and 0.50 NA values.

| Lens NA | α coefficient | β coefficient | Phase plate sag (µm) |
|---------|----------------------|---------------|----------------------|
| 0.25 | 5.754e-8 | 1 | 5.6 |
| 0.33 | 7.138e-8 | 1 | 7.1 |
| 0.50 | 5.794e-7 | 0 | 40.6 |

2.2. Variable logarithmic phase plates: design approach and results

As discussed above, researchers have previously demonstrated the use of an analytical method to derive the freeform surface equation of a phase plate pair that generates a desired wavefront deformation through relative lateral shifts [27,43]. In this approach, the wavefront deformation is proportional to the derivative of the freeform surface in the phase plate pair and the relative shift amount between the pair. However, this approach cannot solve for wavefront deformations caused by mathematical surface descriptions and derivatives with interdependent terms and parameters. In our case, the composite surface created by the shifted VLPPP includes logarithmic and XY-polynomial interdependent terms that are not conducive to analytic integration. As a consequence, we apply the numerical approach demonstrated in Ref. [43] for the VLPPP design. In this approach, two boundary elements are defined in the form of point clouds, along with the desired relative shift for the phase plate pair, to design variable freeform elements utilizing numerical integration techniques.

For the present work, the boundary elements are the LPPs designed for the 0.25 and 0.5 NA aspheric singlets, and the maximum desired shift between the phase plate pair is set as ± 2 mm. The relative shift between the phase plate pair components is chosen based on the required clear aperture, manufacturing constraints, and opto-mechanical requirements. The boundary surface diameters are set by adding at least twice the maximum desired shift amount between the pair to their clear apertures to ensure all rays transmit through the surfaces. For this example, a 26 mm aperture was divided into 501×501 sample points. After calculating the required VLPPP surfaces, the relative shift required to enable EDoF for the 0.33 NA lens was calculated by minimizing the difference between the composite surface from the VLPPP as surfaces were incrementally shifted to the LPP designed for 0.33 NA lens. The point clouds representing VLPPP surfaces were then implemented in CODE V as NURBS surfaces, which allow for implementing height maps with unequal spacing as the base optical surface with no need to define conventional surface properties (radius of curvature, conic constant, etc.) [44,45].

The VLPPP surfaces were then shifted to quantify the performance of the system. Figure 1(b) shows the schematic of the 0.25 NA aspheric lens with shifted VLPPP as an example. The three fixed LPPs are thus replaced by one VLPPP. Table 3 summarizes the shifts required to enable EDoF for each aspheric lens, and Fig. 4 shows a 3D plot of one of the VLPPP surfaces.

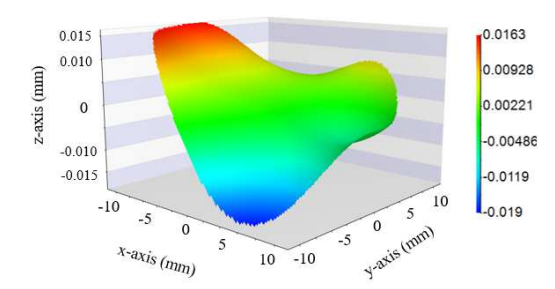


Fig. 4. 3D surface map of one of the variable logarithmic phase plates over 22 mm clear aperture.

Table 3. VLPPP design results.

| Lens NA | Relative phase plate shift (mm) | Phase plate sag (µm) |
|---------|---------------------------------|----------------------|
| 0.25 | -2 | |
| 35.3 | 0.33 | 0.44 |
| 0.50 | 2 | |

3. LPP and VLPPP performance analysis

3.1. On-axis system performance

This section analyzes the on-axis performance of the LPPs and VLPP by considering both rayand wave-based models.

3.1.1. Through-focus spot diagrams

Figure 5 qualitatively compares the through-focus spot diagrams for the three lenses with and without the LPP and VLPPP. As expected, the spot sizes increase with the addition of phase plates, with smaller variation over the designed range of focus ($-6\Delta z$ to $+6\Delta z$). The VLPPP systems create larger spots compared to the LPP designs. More quantitative comparisons are presented below.

3.1.2. Through-focus MTF

As discussed in Sec. 2, the addition of EDoF phase plates decrease system sensitivity to defocus at the expense of reduced resolution. Figure 6 shows the tangential MTF at best focus for all the lenses with and without LPP and VLPPP. With the addition of EDoF phase plates, the on-axis MTF worsens at the best image plane for both phase plates, with LPP performing better than VLPPP, particularly for lower NA lenses.

To illustrate the through-focus on-axis performance of the designed phase plates, Fig. 7 represents the through-focus tangential modulation values for all the lenses with and without EDoF phase plates at 80 cycles/mm as an example. The through-focus variation of the MTF decreases with the addition of the phase plates. The peak MTF values are also lower, as expected.

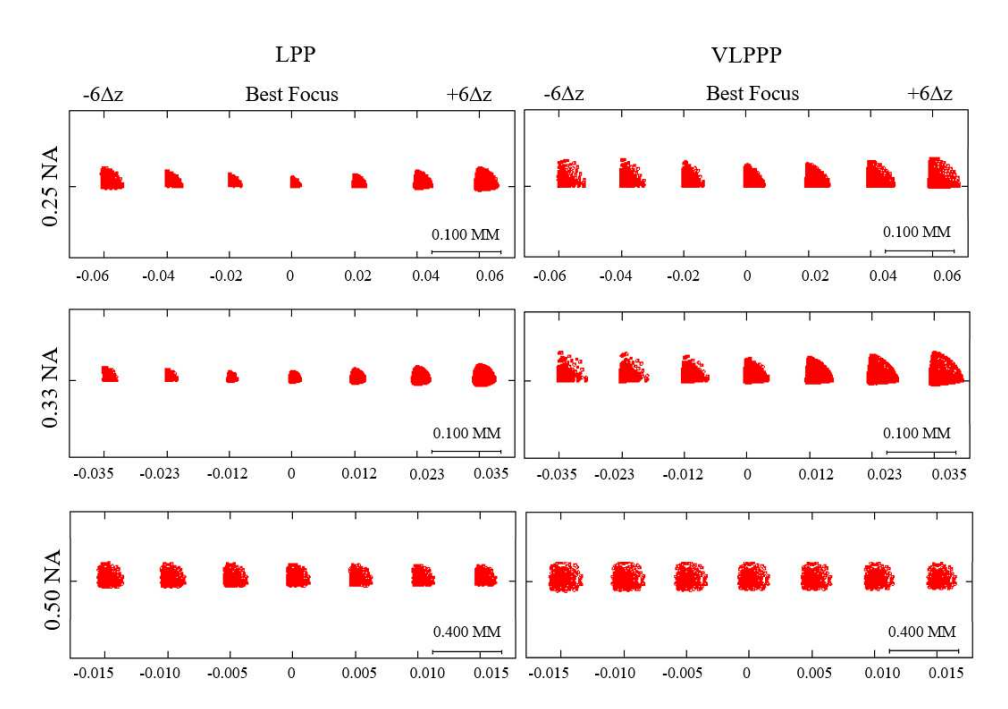


Fig. 5. Through-focus spot diagrams for 0.25, 0.33, and 0.50 NA lenses with LPP and VLPPP.

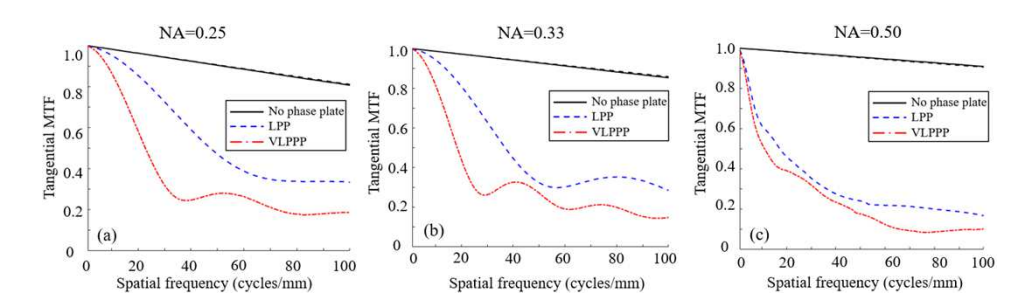


Fig. 6. Tangential MTF at the best focus for the (a) 0.25, (b) 0.33, and (c) 0.50 NA lenses with and without EDoF phase plates.

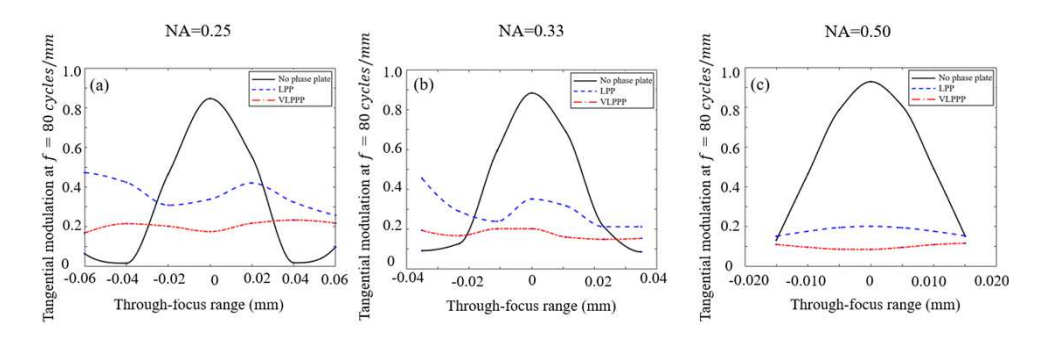


Fig. 7. On-axis through-focus tangential MTF plots (at f = 80 cycles/mm) for the (a) 0.25, (b) 0.33, and (c) 0.50 NA lenses with and without LPPs and VLPPP.

3.1.3. Root-mean-square (RMS) deviation of PSF and slope of RMS deviation of PSF

To qualitatively analyze the effect of EDoF phase plates on system performance, we consider the through-focus PSF variation by calculating the RMS deviation of PSF and its slope introduced previously [42]. For the RMS deviation of PSF calculation, the normalized PSF at best focus and defocus image planes are used to find the RMS values, following Eq. (3):

$$RMS = \sqrt{\frac{1}{m^2} \sum_{i=1}^{m} \sum_{j=1}^{m} (PSF_{d,i,j} - PSF_{f,i,j})^2}.$$
 (3)

In Eq. (3), m^2 is the total number of samples in the PSF matrix and $PSF_{d,i,j}$ and $PSF_{f,i,j}$ are the normalized PSF (in matrix form and m = 1024) at the defocused and best focus planes, respectively. The slope of RMS deviation of PSF calculation, which represents the rate at which the RMS deviation of PSF changes through focus, is calculated as follows:

$$s_i = \frac{RMS_{i+1} - RMS_i}{d_{i+1} - d_i}, i = 1, 2, \dots, 6,$$
(4)

where RMS_{i+1} and RMS_i are the RMS deviations of PSF values calculated for the image planes at d_{i+1} and d_i locations respectively, and s_i is the slope of the RMS deviation of PSF for each two consecutive defocus image planes. With the addition of EDoF phase plates, smaller RMS values are expected, which confirms less through-focus variation in PSF. As an example, Fig. 8 shows the normalized PSFs using diffraction-based models for the 0.33 NA lens with its respective shifted VLPPP at best focus and $\pm 4\Delta z$ image plane locations.

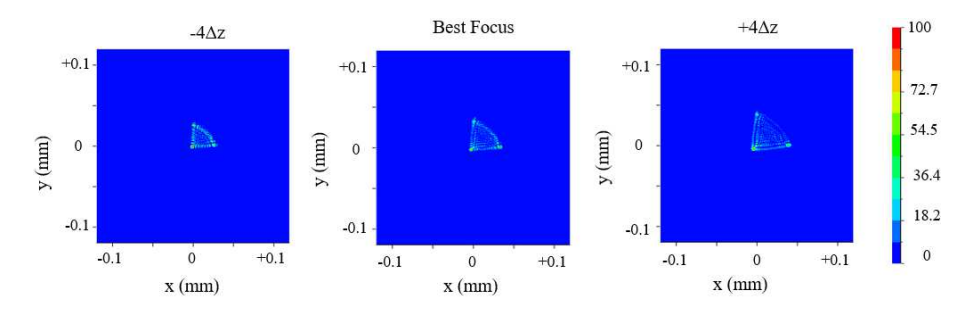


Fig. 8. Normalized PSFs for the 0.33 NA lens with its respective shifted VLPPP at best focus and $\pm 4\Delta z$ image plane locations.

Based on literature [13,18], the LPP enables EDoF over a larger defocus range and therefore, the axial ranges over which the RMS deviation of PSFs are calculated are extended to study phase plate performance. Figure 9 compares the RMS deviation of PSF and its slope for the three lenses with and without LPP and VLPPP over defocus range of $-10\Delta z$ to $+10\Delta z$. With the addition of LPP and VLPPP, the RMS deviation of PSF shows smaller values and the slope of the RMS deviation of PSF exhibits lower values and through-focus variation, confirming more consistent through-focus performance. Since the addition of VLPPP introduces more surfaces and thickness in the optical system, lower performance is expected compared to the equivalent LPP. This behavior is more pronounced in the lower NA systems. The LPP and its equivalent shifted VLPPP show similar performance for the 0.50 NA lens.

3.2. Off-axis system performance

For imaging applications, it is also essential to consider system performance for off-axis object location. This section considers and compares the performance of the designed LPPs and VLPPP over a 3-degree field along the y-axis, as shown in Fig. 10.

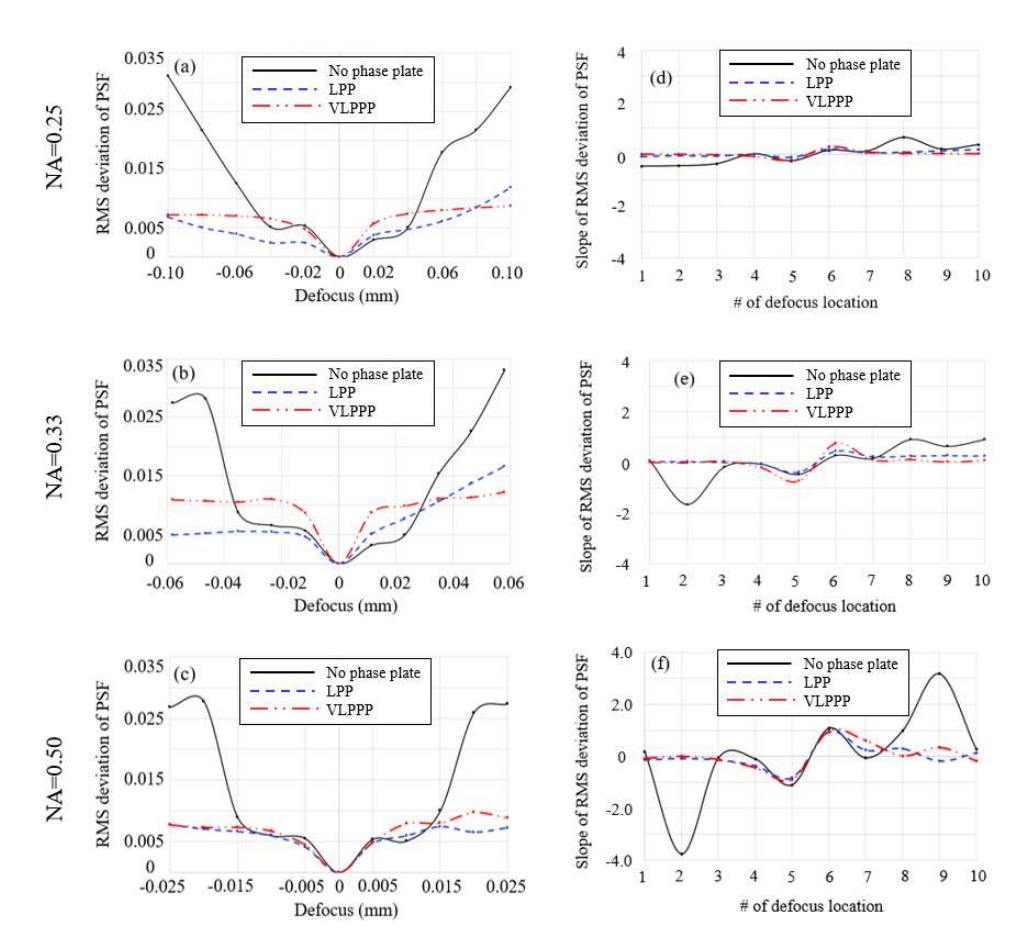


Fig. 9. RMS deviation of PSF through-focus and its slope for (a,d) 0.25, (b,e) 0.33, and (c,f) 0.50 NA lenses with and without the LPP and VLPPP.

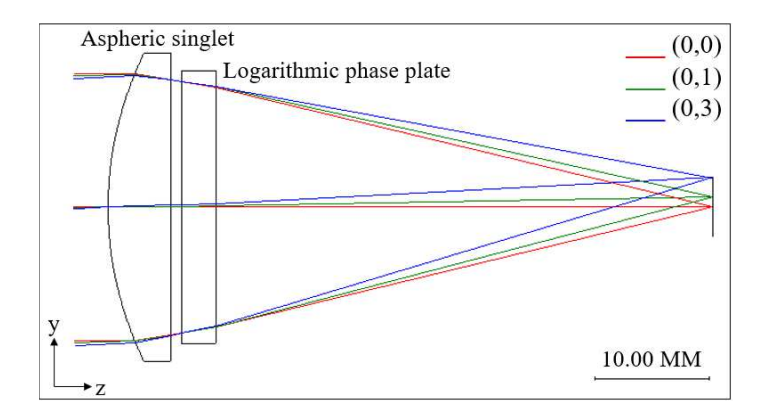


Fig. 10. Location of field angles along the y-axis.

3.2.1. Through-focus spot diagrams vs field angle

We consider the through-focus spot diagrams (ray-based models) for the 0.33 NA lens as an example. As the field angle increases along the y-axis, the spot sizes and shapes for the LPP and VLPPP change (Fig. 11). The location of the smallest spot also changes at higher field angles which is expected due to field dependent aberrations. This performance trend is also observed for the 0.25 and 0.50 NA lenses with LPP and VLPPP.

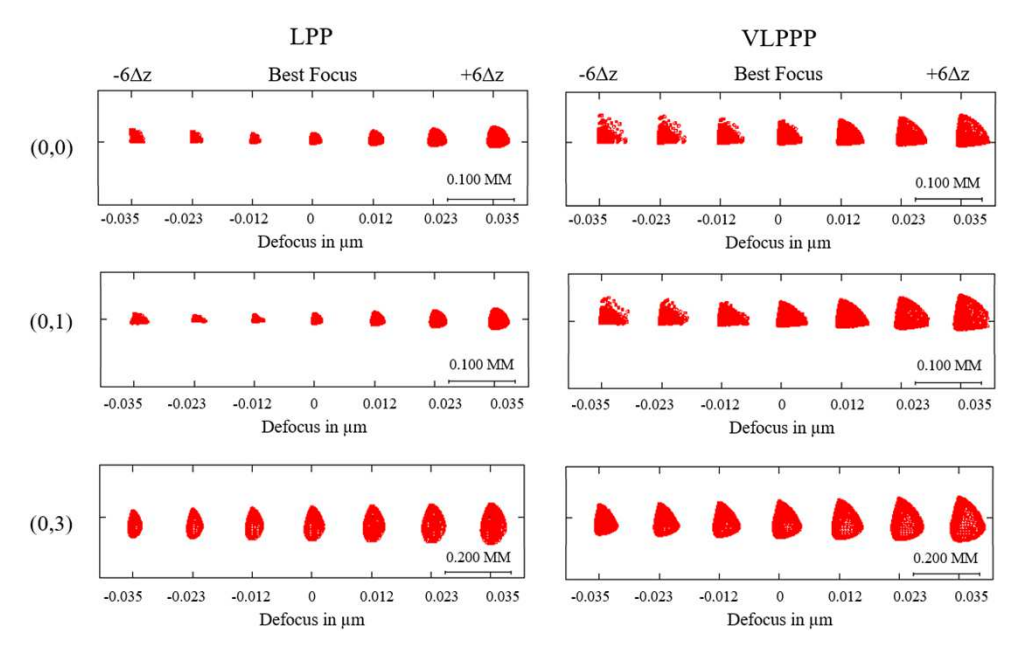


Fig. 11. Through focus spot diagrams (from $-6\Delta z$ to $+6\Delta z$) for the 0.33 NA lens with LPP and VLPPP over a 3-degree field angle along the y-axis

3.2.2. MTF vs field angle

As mentioned previously, system performance degrades with an increase in field angle. As an example, we consider tangential MTF plots at best focus for the 0.33 NA lens with and without the EDoF phase plates at the discussed field points (Fig. 12). At higher field angles, the MTF value decreases overall, worsening the system's performance. This is expected due to the on-axis nature of the optimization routine discussed in Sec. 2. The comparison in Fig. 12 also shows the performance for the 0.33 NA lens with VLPPP at (0,0) and (0,1) degree field points is very similar, with the higher field angle point performing slightly better at some frequencies.

Since it is expected to observe less through-focus MTF variation with the addition of EDoF phase plates, we consider the through-focus tangential modulation plots for the 0.33 NA lens with and without EDoF phase plates over the 3-degree field angle in Fig. 13. As expected, at higher field angles the location of the best image plane changes, resulting in a shift in the maximum modulation value location which becomes less pronounced at higher field angles due to lower overall performance. However, the addition of phase plates leads to less modulation variation.

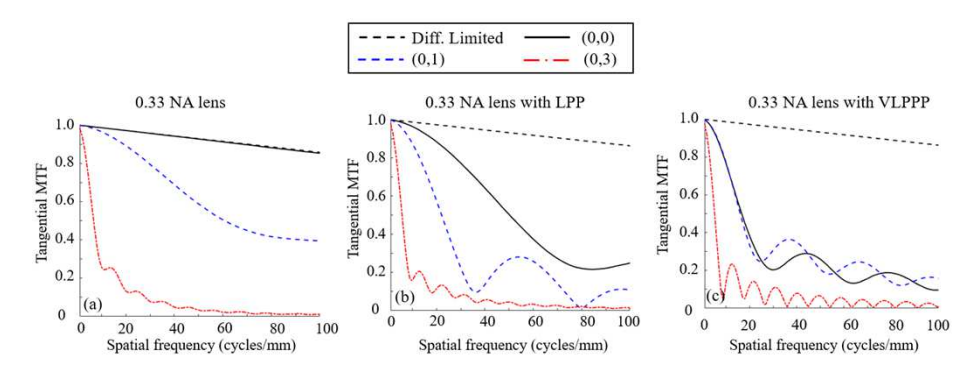


Fig. 12. MTF at best focus for (a) 0.33 NA lens, (b) 0.33 NA lens with LPP and (c) 0.33 NA lens with VLPPP over a 3-degree field angle along the y-axis.

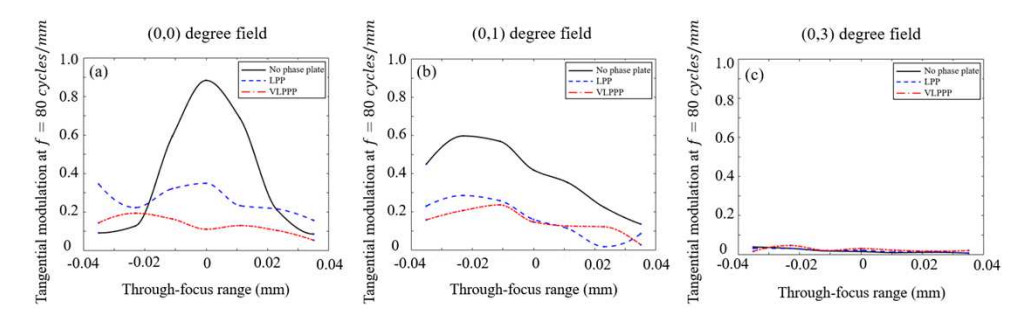


Fig. 13. Through-focus tangential modulation at f = 80 cycles/mm for 0.33 NA lens with and without EDoF phase plates at (a) (0,0), (b) (0,1), and (c) (0,3) field angles along the y-axis.

4. LPP and VLPPP performance comparison to CPP and QPPP

As discussed previously, LPPs have been reported to enable EDoF in imaging systems over a larger range of defocus compared to CPPs designed for the same imaging systems [13,18]. Therefore, as an example, we compare the through-focus spots and RMS deviation of PSF of the previously designed CPPs and QPPP [42] with the current LPPs and VLPPP over a larger range of defocus ($\pm 10\Delta z$). Figure 14 compares the through-focus spot diagrams for the 0.33 NA lens with and without CPP and LPP as an example. With the addition of the EDoF phase plates, the through-focus spots become larger and less sensitive to defocus qualitatively.

Figure 15 compares the RMS deviation of PSF values for the 0. 25, 0.33, and 0.50 NA lenses with and without CPPs, LPPs, QPPP and VLPPP. All phase plates are designed for the same lens and with the same optimization goals, and the only differences are the surface descriptions of the phase plates. For the lower NA lenses (0.25 and 0.33), the CPPs perform similar to or slightly better than the LPPs. For the highest NA lens, the CPP has lower RMS deviation of PSF over the designed range of defocus, suggesting a consistent through-focus performance. However, the LPP RMS values decrease or are closer to the RMS value for the designed CPP for |defocus|>6 Δz . This suggests that the LPP can enable EDoF for higher NA lenses and over a larger range of defocus compared to CPP. For the VLPPP and QPPP performance comparison, Fig. 15 shows that the RMS deviation of PSF values are smaller for the QPPP for the lower NA lenses, creating more consistent through-focus spots compared to VLPPP. For the highest NA lens, the QPPP and VLPPP comparison show that over the designed range of defocus, QPPP has a smaller RMS deviation of PSF, and over a larger range defocus range, the VLPPP performs better only on one

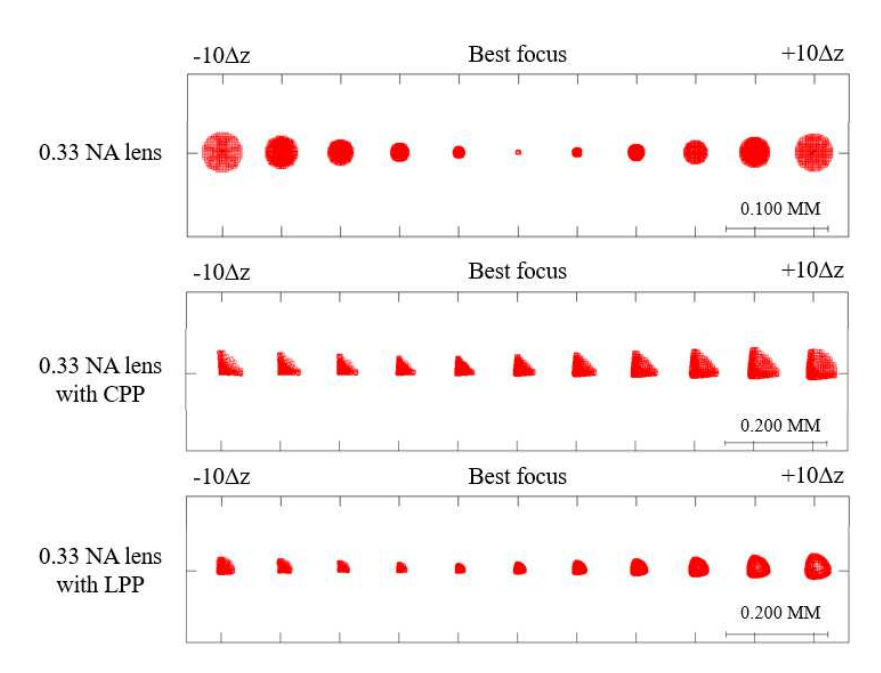


Fig. 14. Through-focus $(-10\Delta z \text{ to } + 10\Delta z)$ spot diagrams for the 0.33 NA lens with and without the EDoF phase plates.

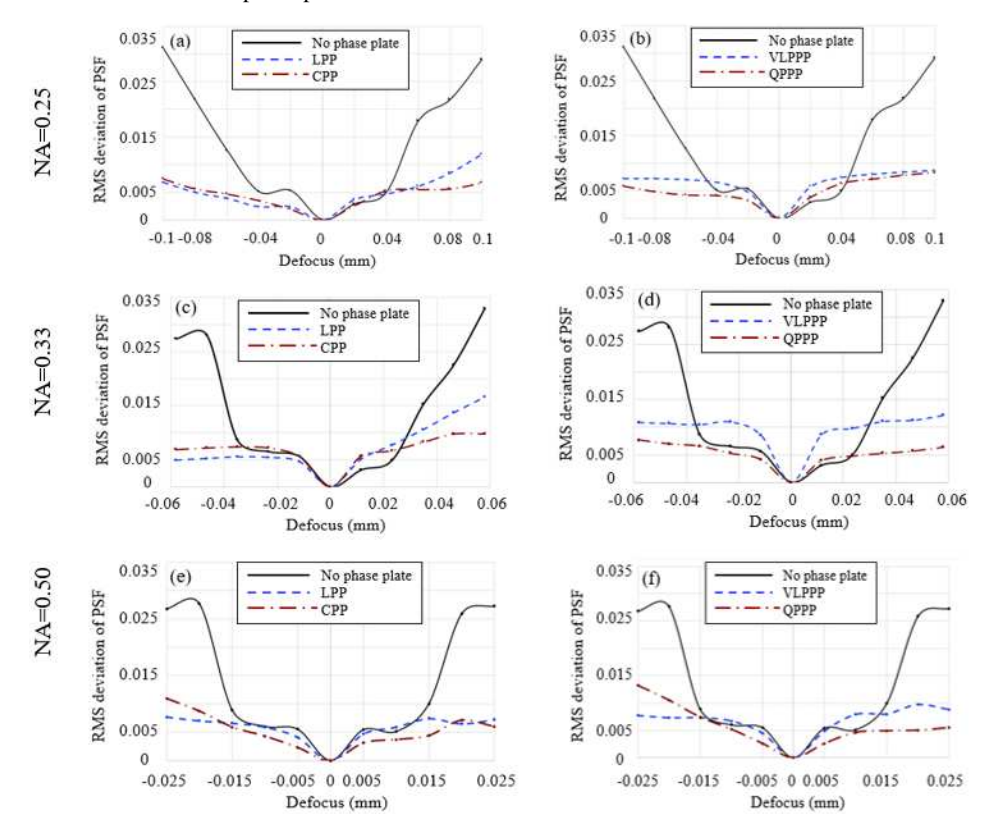


Fig. 15. Comparison of RMS deviation of PSF between previously designed CPP and QPPP with current LPP and VLPPP designs for (a,b) 0.25, (c,d) 0.33, and (e,f) 0.50 NA lenses.

side of the focus. However, the slope of the RMS deviation of PSF through-focus for the highest NA lens with VLPPP is smaller compared to QPPP. Therefore, for higher NA lenses and over large ranges of defocus, VLPPP could be advantageous due to its ability to create less and/or slow varying PSFs compared to the QPPP.

5. Discussion and conclusion

In this paper, we have proposed a method to design a phase plate pair that enables variable extended depth of field through relative translation of the phase components using a numerical design approach. Three fixed phase plates with logarithmic surface description were designed initially for commercial lenses with different NA values. The motivation for selection of logarithmic surface type was its reported capability to enable EDoF over a larger defocus range compared to the CPPs. The LPP surface parameters were optimized to meet two design goals: (1) improving on-axis system MTF by increasing the MTF values at specific spatial frequencies and (2) decreasing on-axis MTF variation through focus by minimizing the MTF differences at the selected frequencies. One VLPPP then replaced three LPPs to enable EDoF for the baseline lenses. For the VLPPP design a numerical method was used instead of an analytical approach. The need for use of the numerical approach was rooted in logarithmic and XY-polynomial interdependent terms in the surface description of the LPP. This method leverages numerical integration (developed in MATLAB) to find the required variable surfaces. The implementation of the LPPs required user-defined surfaces and the VLPPP was implemented using NURBS user-defined surfaces in CODE V.

The performance of the designed EDoF phase plates (LPPs and VLPPP) were considered for both ray- and wave-based models and on- and off-axis rays. The through-focus spot diagrams qualitatively showed that with the addition of the LPPs and VLPPP, the on-axis spots become larger and less sensitive to defocus. A similar comparison over the 3-degree field angle (along the y-axis) showed that the spot sizes and shapes vary through field and the location of the smallest spot shifts at higher field angles due to the presence of field-dependent aberrations such as field curvature. These comparisons confirmed that both LPPs and VLPPP enable focus-invariant systems, with their best performance on-axis.

As a quantitative metric, we also compared the RMS deviation of PSF and its slope for the LPPs and VLPPP. These metrics represent the self-similarity of the through-focus PSFs and the rate at which the PSFs change through-focus respectively. As the image plane location moves across the optic axis and away from the nominal best focus in a standard imaging system, the PSF changes and therefore, the RMS deviation of PSF gets larger through focus. With the addition of the LPPs and VLPPP, the RMS deviation of PSF values and their slope were reduced.

The MTF at best focus and through-focus were also studied for each lens with and without EDoF phase plates (on- and off-axis) which showed that system MTF decreases and varies less through-focus with the addition of the phase plates. These observations were consistent for both on- and off-axis fields, with the systems performing worse off-axis which is expected due to the on-axis nature of the optimization routine. The field sensitivity of the system performance can be linked to the asymmetries in the surfaces of the phase plates and the directionality of the shifts between the VLPPP components. Further analyses could be performed on the 2D MTF of the EDoF phase plates and performance metrics such as the Minimum Modulation Curve [46,47]. In addition, optimization methods that consider the off-axis performance of the phase plates have the potential to improve the imaging quality of these systems.

As mentioned previously, the motivation for this work was the suggestion by the literature that the LPP enables EDoF over a larger range of defocus compared to CPP. As a result, a comparison was performed for the through-focus spots and RMS deviation of PSFs for the previously designed CPPs and QPPP with the current LPPs and VLPPP. Our observations showed that for the lower NA lenses, the LPPs and equivalent VLPPP do not offer a great performance advantage over

the CPPs and QPPP. However, for the highest NA lens the performance difference between the CPP and LPP (and the QPPP and VLPPP) is more pronounced and the rate at which the RMS deviation of PSF varies through-focus is smaller. Additional design and optimization are needed to further investigate the LPP and VLPPP performance for lenses with higher NA values.

Funding. NSF I/UCRC Center for Freeform Optics (IIP-1822026, IIP-1822049).

Acknowledgments. The authors would like to acknowledge valuable discussions with Dr. Christoph Menke from Carl Zeiss AG, Dr. Sébastien Héron from THALES, Dr. Glenn Boreman from the University of North Carolina at Charlotte, and Dr. Jannick Rolland from the University of Rochester. The authors would also like to thank Synopsys for the CODE V license used in this work.

Disclosures. The authors declare no conflicts of interest.

Data availability. Data underlying the results presented in this paper are not publicly available at this time but may be obtained from the authors upon reasonable request.

References

- 1. T. S. Tkaczyk, "Field Guide to Microscopy," SPIE Field Guides (SPIE press, Bellimngham, Washington USA, 2010).
- M. Bass, E. W. V. Stryland, D. R. Williams, and W. L. Wolfe, "Handbook of Optics Volume II Devices," Measurements, and Properties 2nd edition (1995).
- 3. E. Dowski and G. Johnson, "Wavefront coding: a modern method of achieving high-performance and/or low-cost imaging systems," *SPIE's International Symposium on Optical Science, Engineering, and Instrumentation* (SPIE, 1999), Vol. 3779.
- 4. W. Chi and N. George, "Electronic imaging using a logarithmic asphere," Opt. Lett. 26(12), 875-877 (2001).
- K. Chu, N. George, and W. Chi, "Incoherently combining logarithmic aspheric lenses for extended depth of field," Appl. Opt. 48(28), 5371–5379 (2009).
- Z. Zhai, S. Ding, Q. Lv, X. Wang, and Y. Zhong, "Extended depth of field through an axicon," J. Mod. Opt. 56(11), 1304–1308 (2009).
- F. Zhou, R. Ye, G. Li, H. Zhang, and D. Wang, "Optimized circularly symmetric phase mask to extend the depth of focus," J. Opt. Soc. Am. A 26(8), 1889–1895 (2009).
- R. N. Zahreddine and C. J. Cogswell, "Binary phase modulated partitioned pupils for extended depth of field imaging," in *Imaging and Applied Optics* 2015, OSA Technical Digest (online) (Optical Society of America, 2015), IT4A.2.
- 9. K. Chu, N. George, and W. Chi, "Extending the depth of field through unbalanced optical path difference," Appl. Opt. 47(36), 6895–6903 (2008).
- J. Ojeda-Castaneda, J. E. A. Landgrave, and H. M. Escamilla, "Annular phase-only mask for high focal depth," Opt. Lett. 30(13), 1647–1649 (2005).
- 11. R. Zahreddine, R. Cormack, and C. Cogswell, "Simultaneous quantitative depth mapping and extended depth of field for 4D microscopy through PSF engineering," in *SPIE BiOS*, (SPIE, 2012),
- E. R. Dowski and W. T. Cathey, "Extended depth of field through wave-front coding," Appl. Opt. 34(11), 1859–1866 (1995)
- S. S. Sherif, W. T. Cathey, and E. R. Dowski, "Phase plate to extend the depth of field of incoherent hybrid imaging systems," Appl. Opt. 43(13), 2709–2721 (2004).
- G. Carles, "Analysis of the cubic-phase wavefront-coding function: Physical insight and selection of optimal coding strength," Opt. Lasers Eng. 50(10), 1377–1382 (2012).
- J. van der Gracht, E. R. Dowski, M. G. Taylor, and D. M. Deaver, "Broadband behavior of an optical-digital focus-invariant system," Opt. Lett. 21(13), 919–921 (1996).
- H. Zhao, Q. Li, and H. Feng, "Improved logarithmic phase mask to extend the depth of field of an incoherent imaging system," Opt. Lett. 33(11), 1171–1173 (2008).
- H. Zhao and Y. Li, "Performance of an improved logarithmic phase mask with optimized parameters in a wavefrontcoding system," Appl. Opt. 49(2), 229–238 (2010).
- S. Sherif, E. Dowski, and W. T. Cathey, "Logarithmic phase filter to extend the depth of field of incoherent hybrid imaging systems," in *International Symposium on Optical Science and Technology*, (SPIE, 2001),
- S. Prasad, T. Torgersen, V. Pauca, R. Plemmons, and J. van der Gracht, "Engineering the pupil phase to improve image quality," in AeroSense 2003, (SPIE, 2003),
- 20. S. Bagheri, P. Silveira, R. Narayanswamy, and D. Pucci de Farias, "Design and optimization of the cubic-phase pupil for the extension of the depth of field of task-based imaging systems," in SPIE Optics + Photonics, (SPIE, 2006),
- 21. L. W. Alvarez, "Two-element variable-power spherical lens," U.S. 3(305), 294 (1967).
- M. Bawart, A. Jesacher, P. Zelger, S. Bernet, and M. Ritsch-Marte, "Modified Alvarez lens for high-speed focusing," Opt. Express 25(24), 29847–29855 (2017).
- 23. A. W. Lohmann, "A New Class of Varifocal Lenses," Appl. Opt. 9(7), 1669–1671 (1970).
- 24. S. Barbero, "The Alvarez and Lohmann refractive lenses revisited," Opt. Express 17(11), 9376–9390 (2009).

- 25. J. A. Shultz and T. J. Suleski, "Design of a Variable Toric Lens Using Laterally Shifted Freeform Elements," in Optical Design and Fabrication 2017 (Freeform, IODC, OFT), OSA Technical Digest (online) (Optica Publishing Group, 2017), JW2C.2.
- 26. M. Bawart, A. Jesacher, S. Bernet, and M. Ritsch-Marte, "Remote focusing in confocal microscopy by means of a modified Alvarez lens," J. Microsc. 271(3), 337–344 (2018).
- 27. I. A. Palusinski, J. M. Sasián, and J. E. Greivenkamp, "Lateral-shift variable aberration generators," Appl. Opt. 38(1), 86-90 (1999).
- 28. T. Mitchell and J. Sasian, "Variable aberration correction using axially translating phase plates," AeroSense '99 (SPIE, 1999), Vol. 3705.
- 29. E. Acosta and S. Bará, "Variable aberration generators using rotated Zernike plates," J. Opt. Soc. Am. A 22(9), 1993-1996 (2005).
- 30. S. Shadalou, W. J. Cassarly, and T. J. Suleski, "Tunable illumination for LED-based systems using refractive freeform arrays," Opt. Express 29(22), 35755-35764 (2021).
- 31. T. Suleski, J. Shultz, and P. Smilie, "Dynamic beam shaping with freeform optics," SPIE Optical Engineering + Applications (SPIE, 2014), Vol. 9194.
- 32. P. J. Smilie and T. J. Suleski, "Variable-diameter refractive beam shaping with freeform optical surfaces," Opt. Lett. **36**(21), 4170–4172 (2011).
- 33. T. Hellmuth, A. Bich, R. Börret, A. Holschbach, and A. Kelm, "Variable phaseplates for focus invariant optical systems," in Optical Systems Design 2005, (SPIE, 2005),
- 34. J. Ojeda-Castañeda, E. A. Gomez, H. P. Mora, M. T. Cisneros, E. R. Ledesma Orozco, J. S. Pacheco Santamaria, J. G. Martinez Castro, and R. C. Salas Segoviano, "Optical System With Variable Field Depth," U.S. 8,159,753 B2 (2012).
- 35. J. Ojeda-Castañeda and C. M. Gómez-Sarabia, "Tuning field depth at high resolution by pupil engineering," Adv. Opt. Photonics 7(4), 814-880 (2015).
- 36. J. Ojeda-Castañeda, J. E. A. Landgrave, and C. M. Gómez-Sarabia, "Conjugate phase plate use in analysis of the frequency response of imaging systems designed for extended depth of field," Appl. Opt. 47(22), E99-E105 (2008).
- 37. A. Castro and J. Ojeda-Castañeda, "Asymmetric phase masks for extended depth of field," Appl. Opt. 43(17), 3474-3479 (2004).
- 38. L. Ledesma-Carrillo, R. Guzmán-Cabrera, C. M. Gómez-Sarabia, M. Torres-Cisneros, and J. Ojeda-Castañeda, "Tunable field depth: hyperbolic optical masks," Appl. Opt. 56(1), A104-A114 (2017).
- 39. M. Demenikov, G. Muyo, and A. R. Harvey, "Experimental demonstration of continuously variable optical encoding in a hybrid imaging system," Opt. Lett. 35(12), 2100-2102 (2010).
- 40. S. S. Rege, T. S. Tkaczyk, and M. R. Descour, "Application of the Alvarez-Humphrey concept to the design of a miniaturized scanning microscope," Opt. Express 12(12), 2574–2588 (2004).
- 41. "Edmund Optics", retrieved https://www.edmundoptics.com/f/precision-aspheric-lenses/13139.
- 42. S. Moein and T. J. Suleski, "Freeform optics for variable extended depth of field imaging," Opt. Express 29(24), 40524-40537 (2021).
- 43. S. Shadalou and T. J. Suleski, "General design method for dynamic freeform optics with variable functionality," Opt. Express 30(11), 19974-19989 (2022).
- 44. "CODE V Lens System Setup Reference Manual," (2021).
- 45. "User-defined features in CODE V," (2009).
- 46. H. Aryan, G. D. Boreman, and T. J. Suleski, "The Minimum Modulation Curve as a tool for specifying optical performance: application to surfaces with mid-spatial frequency errors," Opt. Express 27(18), 25551–25559 (2019).
- 47. G. D. Boreman, "Modulation transfer function in optical and electro-optical systems," Tutorial texts in optical engieering (SPIE), Vol. TT121.